Nuclear Engineering and Technology 52 (2020) 2025–2033

Contents lists available at ScienceDirect

Nuclear Engineering and Technology

journal homepage: www.elsevier.com/locate/net

Original Article

Lab scale electrochemical codeposition experiments for comparison to computational predictions

Philip Lafreniere [a], Chao Zhang [b], Michael Simpson [b], Edward D. Blandford [a, *]

[a] Department of Nuclear Engineering, University of New Mexico, MSC01 1120, 1 University of New Mexico, Albuquerque, NM, 87131, USA
[b] Department of Metallurgical Engineering, University of Utah, WBB 412, Salt Lake City, UT, 84112, USA

ARTICLE INFO

Article history:
Received 18 January 2019
Received in revised form
6 January 2020
Accepted 10 February 2020
Available online 11 February 2020

Keywords:
Pyroprocessing
Signature-based safeguards
Experimental validation
Electrochemical modeling

ABSTRACT

Signature-based safeguards (SBS) is being developed to assist tradition nuclear material accountancy methods in tracking material in pyroprocessing facilities. SBS involves identifying off-normal scenarios that would result in improper movement of material in a pyroprocessing facilities and determining associated sensor response signatures. SBS investigations are undertaken in the computational space utilizing an electrochemical transport code known as enhanced REFIN with anodic dissolution (ERAD) to calculate the affect of off-normal conditions in the electrorefiner (ER) on material movement. Work is undertaken to experimentally validate the predictions and assumptions made by ERAD for off-normal occurrences. These experiments were undertaken on a benchtop scale and involved operating an electrochemical cell at 10 separate current densities for constant current operations to deposit U and Gd at a W cathode. These experiments were then modeled using ERAD to compare calculated predictions versus analytical experimental results it was found. It was discovered both the experimental and calculated results reflect a trend of increased codeposition of U and Gd with increasing current density. ERAD was thus demonstrated to be useful for predicting trends from anomalous operation but will require further optimization to be utilized as a quantitative design tool.

1. Introduction

Pyroprocessing has long been investigated as a potential commercial method of recycling used nuclear fuel (UNF). This technology utilizes electrochemical methods to separate actinides from used nuclear fuel to generate fuel ingots and pins suitable for use as fuel in fast spectrum metal fuel reactors. The methods have to date been developed on the engineering scale at the Fuel Conditioning Facility (FCF) at the Idaho National Laboratory (INL) and the Pyroprocess Integrated Inactive Demonstration Facility (PRIDE) at the Korea Atomic Energy Research Institute (KAERI) [1,2]. Actual spent fuel from Experimental Breeder Reactor-II (EBR-II) has been processed in FCF, while PRIDE has been used to process simulated spent fuel containing depleted U and fission product surrogates. Pyroprocessing has several advantages in that it can process fuel at higher burnups and requires a smaller facility compared to alternative recycling methods such as PUREX aqueous reprocessing. This makes pyroprocessing attractive to nations looking to reduce the actinide disposal demands of a long-term geologic repository. Despite these advantages, pyroprocessing, like aqueous reprocessing, faces several challenges when trying to meet international safeguards requirements [2].

The International Atomic Energy Agency (IAEA) defines safeguards as, “Activities carried out to establish the quantities of nuclear material present within defined areas and the changes in those quantities within defined periods [3].” In particular to reprocessing, the ability to determine the content of Pu present with low uncertainty to determine that a significant quantity (SQ) has been diverted is challenging utilizing traditional mass balance techniques. This is due to a combination of the high throughput of Pu and the limitations of mass quantification and sampling techniques [4]. Pyroprocessing faces additional unique challenges in that it does not possess an input accountability tank (IAT) like aqueous reprocessing, thus making initial inventory difficult. An economically viable plant cannot be flushed regularly for safeguards purposes as the actinide concentration in the electrorefiner must remain at steady state for long term commercial operation [2]. To address these issues, methods involving process monitoring (PM) are being developed to provide assistance to the typical mass balance techniques.

* Corresponding author.
E-mail address: edb@unm.edu (E.D. Blandford).

https://doi.org/10.1016/j.net.2020.02.005

PM methods utilize process measurements to determine if a facility is operating in a normal expected mode or an off-normal mode that would imply the diversion is occurring. These safeguard significant off-normal operations comprise both diversion scenarios and failure modes with safeguard implications [4–6]. These failure modes are of particular significance as they can be reasonably expected to happen and if they do can result in flow of actinides in the material flow sheet to locations that are not intended. For example, Pu depositing at the U cathode resulting in Pu in the U cathode product. One p.m. method that has been the subject of significant investigation is known as Signature Based Safeguards (SBS) [6–8]. SBS utilizes a systems-based method to combine data signals from various unit operations to determine the presence of off-normal operations and to identify their nature. To adequately perform SBS, failure modes must be identified and their expected change in operating signals from process measurements determined. Thus, current work in SBS has taken two forms: identification of failure modes and associated sensors and the determination of normal and off normal data signals for these identified failure modes. The majority of past work with data signal determination in SBS has occurred within the computational space.

Past computational work with SBS has utilized the application of the electrochemical transport code Enhanced REFIN with Anodic Dissolution (ERAD) [6,9,10]. ERAD allows for the simulation of both postulated normal and off-normal operations of the pyroprocessing electrorefiner (ER) [11,12]. These studies focused on three failure modes that could result in codeposition and production of a Pu and U product as opposed to a desired pure U metal ingot. Failure modes of focus were change in cathode surface area, change in diffusion layer thickness due to change in rotational speed of electrode, and poorly quantified feedstock of material in the anode basket [6]. These three failure modes all potentially lead to the codeposition of Pu and U, and measurable signals from both voltammetric measurements and neutron counting measurements of the final ingot were simulated. These simulations demonstrated that codeposition can occur under specific conditions for these failure modes, and they could potentially be detected via PM of the facility's unit operations [6].

The results from these studies have considerable qualitative merit, but require significant research to be viewed as having quantitatively accurate results. This is due to ERAD not being experimentally validated at any level whether it is on the engineering scale or the bench top scale. The objective of this paper's study is to generate data from lab scale experiments to support validation of the conclusions drawn from ERAD calculations. In particular it focuses on results for expected surrogate mass depositions and electrochemical signals calculated from ERAD. The specific failure mode investigated in this paper is that of change in cathode surface area.

2. ERAD electrorefiner model

Preliminary studies involving computational modeling of pyroprocessing unit operations and their related safeguards equipment have demonstrated that computational related research can potentially provide assistance in the development of safeguards systems for pyroprocessing facilities. However, the computational models for one of the key pyroprocessing steps, electrorefining, have yet to be experimentally validated. One computational model used in multiple studies, and most significantly in SBS development, is ERAD [6,9]. Validating the predictions made by ERAD is key to future conclusions produced by computational studies simulating commercial pyroprocessing operations. This validation is both beneficial to the operations and safeguards of a pyroprocessing facility under development.

From the perspective of operations, validation of an electrochemical mass transport model such as ERAD can help inform design and throughput criteria as well as evaluate potential failure modes. Computational models can simulate ER operations at commercial scales to provide insight into what operating conditions will provide best production of U product without codeposition at the U cathode of other TRU products such as Pu. This allows for the actinides in the salt to be treated through salt cleanup methods such as electrowinning (EW), thus making most efficient flowsheet with increased separations of both. In addition, the effects of failure modes within the ER equipment can be evaluated to determine the effects on throughput. Failure modes can lead to a change in ER output and thus change the flowsheet of materials and reduce the total amount of material separated. These mistakes can be costly as the equipment is located within a hot cell environment and thus will require significant downtime in order to correct. These simulations can show best ways to detect these anomalous occurrences. By combining data from both types of studies, the placement of unit operations equipment within facility in terms of number of ER and EW can be determined with failure modes affects accounted for and their frequency through traditional probabilistic risk analysis (PRA) assessment. This constitutes a risk-informed design that reduces the need to retrofit a facility with targeted placement of unit operations and sensing equipment after construction.

In addition, validating ERAD's underlying assumptions can have significant impacts to the safeguards of a facility both in their development and application. Understanding how a system behaves during off-normal operations whether unintentional or intentional is integral to determining methods of detection of these forms of operations. Like with operational improvement, safeguards improve greatly by understanding the disruption in the material flowsheet that comes from off-normal operation. The detectability of these off-normal operations can be inferred. This is an important application for the development of PM sensor systems for safeguards as their detectability can be translated in a manner in which the Probability of Detection is increased [4].

ERAD is a one dimensional electrochemical transport code that utilizes a series of assumptions and fundamental kinetics and dynamics equations to calculate material transport in ER operations. ERAD is a modification of the computer code REFIN with additional coding applied to the issues of anodic geometry and transport of materials in the anode diffusion layer [11, 13, 14].

ERAD solves for mass transfer utilizing a finite element method dividing the ER into cells for five different regions: the anode, the anode diffusion layer, the bulk salt, the cathode diffusion layer and the cathode [13]. This special problem is solved over a specified time period with a specified time step within the input file. The input file takes into account several factors. The first is the solver specifics with regards to the mesh and the time period and steps of the solver. The input file feeds into the ERAD program this data as well as specified elements for transport, the electrochemical parameters of specified elements, the operating parameters, and the initial state and boundary conditions. The elements of transport can be specified, but only a total of ten are allowed and three must always be the elemental constituents of the eutectic (Li, K, and Cl). These other elements are usually a mixture of Zr, rare earth elements and actinides (U and Pu). The specified electrochemical parameters are electrode diffusion layer thickness, exchange current density, standard potentials, valence states, transfer coefficients, and diffusion coefficients. All inputted potentials must be relative to the same reference electrode, which in this case is Cl^-/Cl reference electrode. The initial conditions specified are the temperature, current, concentrations of electrodes and salt, electrode surface area, and initial masses at the electrodes and in the salt.

Within ERAD, these inputs are fed into the primary code REFIN. Within REFIN, these inputs are registered and than an iterative method is utilized for each determined time step calculated from the input file. The iterative method focuses on the same three fundamental calculations. The first calculation made is that of the equilibrium potential of the system for the conditions stated in the input file. This is performed by solving the Nernst equation seen in equation (1).

$$E_{eq,r} = E_{0,r} + \frac{RT}{n_r F}\ln\left(\frac{\gamma X_{ox,i}}{\gamma X_{red,i}}\right) \quad (1)$$

where $E_{eq,r}$ is the equilibrium reduction potential, $E_{0,r}$ is the standard reduction potential, R is the ideal gas constant, T is the temperature, n_r number of electrons transferred, F is the Faraday constant, γ is the activity coefficient, and $X_{ox,i}$ and $X_{red,I}$ are the concentrations of oxidation and reduction of the species *i* in the salt.

Taking the data for equilibrium potential and other electrochemical data from the input file, the second major calculation is that of the partial current densities for the electrodes of the specified species calculated by the Butler-Volmer equation seen in Equation (2).

$$i = i_o\left(\frac{X_{Ox}(0,t)}{X^*_{Ox}}\exp\left(\frac{\alpha nF}{RT}(\eta_r)\right) - \frac{X_{Red}(0,t)}{X^*_{Red}}\exp\left(-\frac{(1-\alpha)nF}{RT}(\eta_r)\right)\right) \quad (2)$$

where i is the species current, i_o is the exchange current density, and α is the transfer coefficient.

The final major calculation made utilizing the calculations for the partial current density is that of the Nernst-Planck equation which calculates the mass transfer rates. The Nernst-Planck Equation is seen in equation (3).

$$\frac{\partial y_i}{\partial t} = -D_i\frac{\partial^2 y_i}{\partial x^2} - \frac{FD_i n_i}{RT}\frac{\partial}{\partial x}y_i\frac{\partial \Phi}{\partial x} \quad (3)$$

where y_i is the concentration of species i, x is the 1D spatial dimension, D_i is the diffusion coefficient of the species i, and the term $\frac{\partial \Phi}{\partial x}$ is the potential gradient.

The work reported in this paper looked to validate the assumptions and underlying calculations of ERAD by generating an analog of previous analysis performed by ERAD within the safeguards application domain. This validation is necessary as ERAD makes several assumptions that simplify the model that may or may not make it accurate when utilizing it to assess an operational scenario. These simplifying assumptions include the fact that it reduces the space to a1-D system as opposed to 3-D, assumes every point along electrode surfaces acts exactly the same, the salt mixture is a perfect homogenous mixture, and a uniform boundary layer that does not fluctuate with time. In particular for the simplification of the geometry into a single dimension, the ER system is divided into a mesh of cells divided into five sections: the solid anode, the solid cathode, the bulk electrolyte salt, a fixed sized anode diffusion/migration layer, and the cathode diffusion/migration layer, and specific to the anode variable size diffusion/migration layer. The solid anode and cathode sections as well as the bulk electrolyte salt are assumed to be a single cell in the x-dimension. The diffusion layers size are set by the programmer but vary between 20 and 200 cells in the x-dimension. Previous work with ERAD applied to safeguards has dealt with the use of process monitoring methods to identify the occurrence of failure modes that have pertinent safeguards effects [6, 7, 16].

The failure mode focused upon in experiments reported in this paper is the change in cathodic surface area. Previous computational calculations determined that with sufficient reduction in cathode surface area, codeposition of Pu and U occurred at the cathode and in significant enough amounts to be determined by analysis with radiation detectors outside of the hot cell [6,10]. In addition, noticeable changes in cathode potential were predicted for the circumstances in which codeposition occurred. This was a result of the cell current being adjusted to a level significantly greater than that could be supported by deposition of only U. Overpotential subsequently increased until co-deposition of U and Pu occurs. Of the three failure modes previously considered, this failure mode was chosen to be replicated due to it being the easiest to perform based on precise adjustment of the control variable. Surface area can be changed by adjusting the immersion depth of the cathode in the salt, which is easily accomplished in an experiment. Concentration and diffusion layer adjustments are deemed to be much more difficult or time consuming to reproduce experimentally.

3. Experimental Setup and methods

All experiments were performed in an argon atmosphere glovebox with oxygen and water both below 0.1 ppm throughout the tests. UCl_3 and $GdCl_3$ (99.99% anhydrous, Alfa Aesar) were dissolved in approximately 50 g of premixed LiCl–KCl eutectic (99.99% anhydrous, SAFC Hitech). The salt mixture was contained in an alumina crucible, which was heated in a Kerr Auto Electro-melt furnace. The salt mixture was maintained at 773 ± 1 K. The temperature was monitored by a thermocouple that measured temperature in the salt and was removed during the runs.

The electrochemical test methods were carried out by a three electrode setup including a working electrode (cathode during constant current deposition), a counter electrode (anode during constant current deposition), and a reference electrode. The working electrode was a W wire 1 mm in diameter. It was attached to a vertical translator (as shown in Fig. 1), which allowed the precise movement of 0.005 mm per step. The counter electrode consisted of U metal sheets that were placed in a stainless steel basket. The reference electrode was an Ag wire (99.9%, Alfa-Aesar) and 5 mol % AgCl (99.9% anhydrous, Strem Chemicals) in LiCl–KCl eutectic in a close ended thin mullite tube. The electrodes were connected to an Autolab PGSTAT302 N potentionstat.

The objective of the experimental study was to validate the calculated effect cathode surface area variations have on the relative amounts of co-deposition of two metals. After mixing and melting the salt in the furnace pictured in Fig. 1, cyclic voltammetry scans were performed with the working electrode fully submerged in the salt to determine the achievable current density (A/cm^2) during deposition experiments. Then a series of constant current deposition runs were performed. For constant current tests, the working electrode served as the cathode, and the counter electrode served as the anode. Changing the immersion depth of the cathode was used to increase or decrease the current density from run to run. The salt mixture used for this study was a combination of LiCl–KCl eutectic, UCl_3 salt (1.3 wt%), and $GdCl_3$ (3.2 wt%).

The alumina crucible with the salt mixture was then placed within the furnace and heated up to a temperature of 530 °C over a period of 2 h. The reference electrode was placed before the heating right above the surface of the eutectic salt. The salt was then determined to be melted and to be at 500 °C through the use of a thermocouple submerged within the eutectic salt mixture. The anode basket, cathode, and reference electrode were then submerged within the melted salt. The reference electrode was only submerged approximately 12 cm into the furnace to allow the tip to

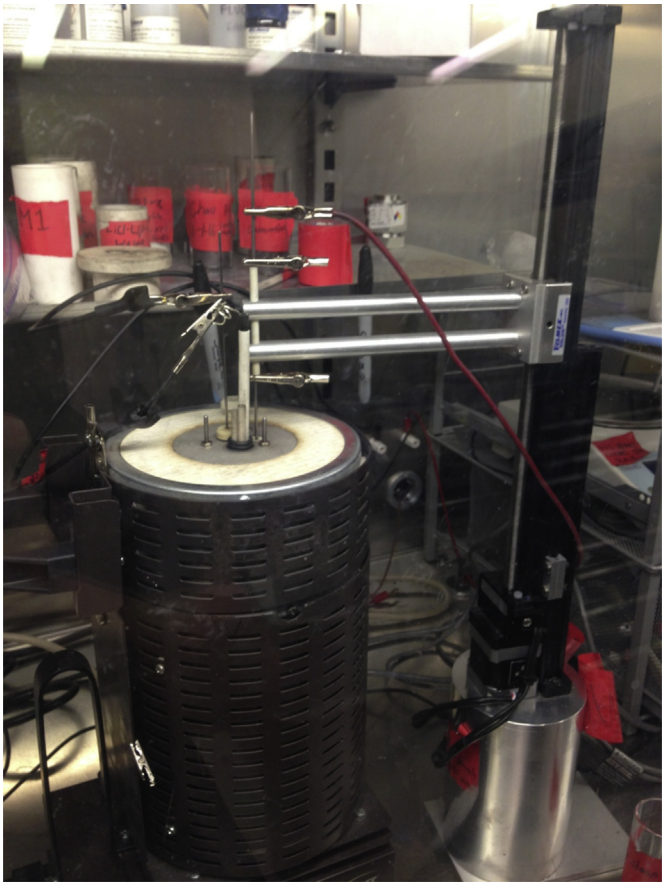

Fig. 1. Experimental Setup featuring a high temperature Kerr furnace, electrodes, and vertical translator.

penetrate the surface of the mixture. The anode and cathode were fully submerged within the salt to touch the bottom of the crucible. The three electrodes were then attached to the leads of the potentionstat.

After a period of about 30 min, the system was assumed to be at thermal equilibrium and CV analysis was performed for two purposes. The first was to determine the salt level in the crucible and to determine the operating currents for the experimental analyses. To determine the salt level, the cathode was raised 1 cm from the bottom of the crucible, and a CV measurement was taken. The Gd reduction peak height was then recorded. The peak height was then recorded in 0.4 cm increments all the way to 3 cm above the bottom of the crucible. The peak height data was then plotted to determine the total salt depth which was estimated to be 31.40 mm. Knowing this, the surface area of the cathode could be adjusted accordingly with regards to submersion depth within the salt.

To determine the operating currents, CV analysis was undertaken at a base working electrode depth of 30.58 mm. The operating current was then identified by inspecting the CV plot. Experiments would be undertaken at two separate currents. The first would be at a current corresponding to the potential just to the left of the Gd peak potential on the CV diagram. The second was a current corresponding to the potential at the start of the Gd peak. With the current and salt depth known, the test matrix for the actual experimental runs could be determined and investigated.

The test matrix of the experimental runs undertaken in this investigation is seen in Table 1. The experimental study consisted of ten constant current runs. Before each run, the cathode wire was adjusted to the surface area desired. CV analysis was then

Table 1
Test matrix for experimental runs.

Run	Current (A)	Time (s)	Depth of Cathode (mm)
1	0.6	60	30.58
2	0.6	60	26.76
3	0.6	60	23.39
4	0.6	60	19.12
5	0.6	60	15.30
A	0.1	60	30.58
B	0.1	60	26.76
C	0.1	60	23.39
D	0.1	60	19.12
E	0.1	60	15.30

performed to “clean” the cathode of any residual or present deposited material by operating the scan at an upper limit potential of 0.4 V. The current was then applied for a total time of 60 s after which there was a 10 s period of which no power was supplied to the cell but measurements for potential were still recorded. Both CV and potential data for these constant current experiments were recorded using the NOVA potentionstat software. After the constant current operation, the cathode was removed from the furnace and the portion of the cathode containing deposits was cut and placed within a sample vial for composition analysis. The cathode was then replaced, and the process was repeated. In addition, before and after each run a salt sample of nominally 0.05 g was taken from the salt.

For composition analysis of both the cathode deposits and salt samples, ICP-MS analysis was utilized. ICP-MS was used to analyze the mass concentrations of U and Gd in all samples. In addition, for Runs 1–5 ICP-MS was used to determine concentrations of Li and K to determine if Li had been reduced at the cathode.

When the cathode was raised out of the salt mixture for sampling, a small amount of the salt inevitably adhered and froze onto the W wire. The salt deposited could not simply be rinsed off with water because there was possibly Li metal deposited that would have reacted with water. Additionally, the metal deposit might not all be tightly packed, therefore there was a risk that some deposit could be rinsed off.

Consequently, the cathode sample sections were each transferred into a beaker with about 26 ml of aqua regia to dissolve all the salt and metal deposit. A small amount of W is expected to dissolve, but that should not interfere with the analysis of Li, K, Gd, and U. The beakers were covered with watch glasses and heated on a hot plate to almost dryness. The beakers were cooled to room temperature then 5 ml HNO_3 and approximately 35 ml ultrapure water was added. Then the beakers were heated to boil and cooled to room temperature. Thereafter, the solutions were collected into a 100 ml volumetric flask and diluted with ultrapure water. Finally, the samples were diluted with 5 vol% HNO_3 to the appropriate dilution for ICP-MS analysis for Li, K, Gd, and U.

The salt samples were directly dissolved into 5 vol% HNO_3 in 100 ml volumetric flasks and diluted for ICP-MS analysis for Li, K Gd, and U. The mass of residual salt on each cathode sample was calculated using the salt composition, deposit weight, and composition.

The sampling of both salt and metal deposits follows the same process for each sample to ensure that the experiment is repeatable. The dilution of the samples is based off of expected compositon from hand calculation to ensure that the concentration falls into the ICP-MS detection range listed for each metals standards. This is a standard laboratory process and is applied to both this experiment as well as other experiments performed at the University of Utah's electrochemical laboratory to ensure repeatable quality of experimental results.

4. Results and analysis

The results from the CV analysis of the salt mixture are seen in Fig. 2. The circles on the plot indicate the operating currents chosen for the subsequent constant current depositions. The currents selected were 0.6 and 0.1 A.

Calculations were performed using ERAD to simulate constant current electrorefining at the conditions of the experiments. Starting concentrations of salt for ERAD input were determined through mass analysis of salt samples that occurred between runs. The diffusion layer thickness for each run was set at 30 μm thick and this value was used for each modeled case. For the setup, this diffusion thickness is chosen as to be significantly larger than that which would be produced by natural convection. In doing so, ERAD captures the changing diffusion layer thickness as it calculates the concentration profile in the diffusion layer. The diffusion layer thickness was determined to be sufficiently large if the concentration profile of the outermost cell of the electrode was constant. The concentration profiles of both electrodes' diffusion layers are calculated and are an output of the code.

Plots of the experimentally measured potentials for each run are seen in Figs. 3 and 4. As expected, the potentials are lower for the 0.6 A runs compared to the 0.1 A runs, for which experiment and model are in agreement. For the 0.6 A depositions, the potential rapidly settles at a value of about −3.3 V. This indicates that Li should be depositing on the cathode along with U and gadolinium based on the CV shown in Fig. 2. For the 0.1 A depositions, potentials initially drop quickly as low as −3.0 V, but all eventually reach a steady value of −2.8 V. Based on the CV in Fig. 2, this indicates that deposition of Gd is occurring with U, but no Li should be depositing.

The results for the calculated potentials from Runs 1–5 and A-E are depicted in Figs. 5 and 6, respectively. While the model does not fit the data values, it does reproduce the effect of cathode surface area. Depth of the cathode decreases from Run 1 to 5, which causes the surface area to decrease. The potential responds by becoming more negative as the area decreases.

It is important to state that the same 50 g mixture of LiCl–KCl–UCl_3-$GdCl_3$ was used for all of the tests from Run 1 through Run 5 and then Run A through Run E. There should be some loss of U and Gd from the mixture as a consequence of electrodeposition. Salt samples were taken before and after each deposition run and analyzed via ICP-MS for U, Gd, Li, and K concentrations. The results are shown in Table 2. It can be seen from the U and Gd concentrations reported in this table that the salt composition remained relatively constant within the statistical variance of the sampling and measurement method. Thus, concentration in the salt can be assumed to be virtually constant during each deposition run. This may partially explain why the modeled potentials are steady with time after the first few seconds as seen in Figs. 5 and 6.

The results of ICP-MS analysis of the metallic deposits on the cathodes are presented in Table 3. The calculated masses for cathode deposits from the ERAD simulations are given in Table 4. Note that the mass of U deposited for each run is much less than the theoretical 25 mg for 0.6 A or 4.2 mg for 0.1 A. This may mean metal fell off of the cathode before it was extracted from the salt. The deposit falling off is evidenced by the plots of potential. It would be expected that the potential would become more positive with time due to the increase of cathode surface area as deposits adhere to the cathode. However, the potential plots exhibit a number of negative spikes of potential indicating that the deposit has fallen into the salt abruptly decreasing the cathode surface area.

Table 4 indicates that the model calculations agree with what was initially expected—less negative cathode potentials (see Figs. 5 and 6) favor U deposition over Gd or Li. The higher the current density, the more Gd and Li should deposit onto the cathode. This same trend is observed experimentally in the results shown in Table 3.

Experimentally, the results are more scattered—presumably due to the likely phenomenon of deposits falling off of the cathode as dendrites. In the low current runs (A-E), the primary metal deposited was U. Relatively small amounts of Gd are deposited, and no Li was detected. In the high current runs (1–5), co-deposition of U, Gd, and Li was detected with exception of run 4 in which Li was not detected. Li measurements may be non-representative, since it forms a liquid metal and likely rises to the surface of the molten salt. The other issue was that analysis of K and Li was used to subtract the estimated salt contribution from each analysis of the deposits. High error for this method can lead to high error in the deduced concentration of metallic Li. Since Li is a major component of the salt, any Li metal on the cathode may be been dominated by Li from the salt. As a result, Li is depositing, but the reported measured Li depositions possess a high uncertainty. This is a result of both the challenges in mass analysis of K in ICP-MS as well as the potential for dissolution of Li into the salt due to it being a liquid and not adhering to the cathode. The dissolution of Li is evident in

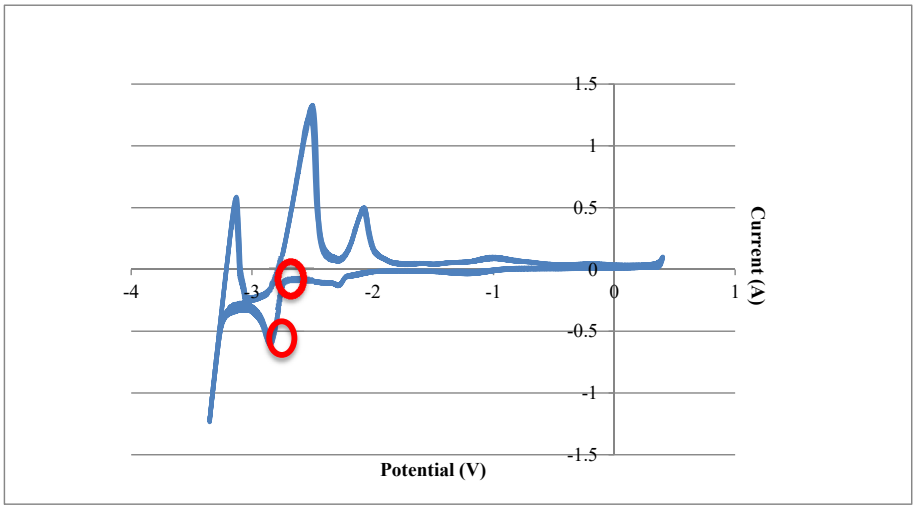

Fig. 2. CV Results with circles indicating where operating currents were selected.

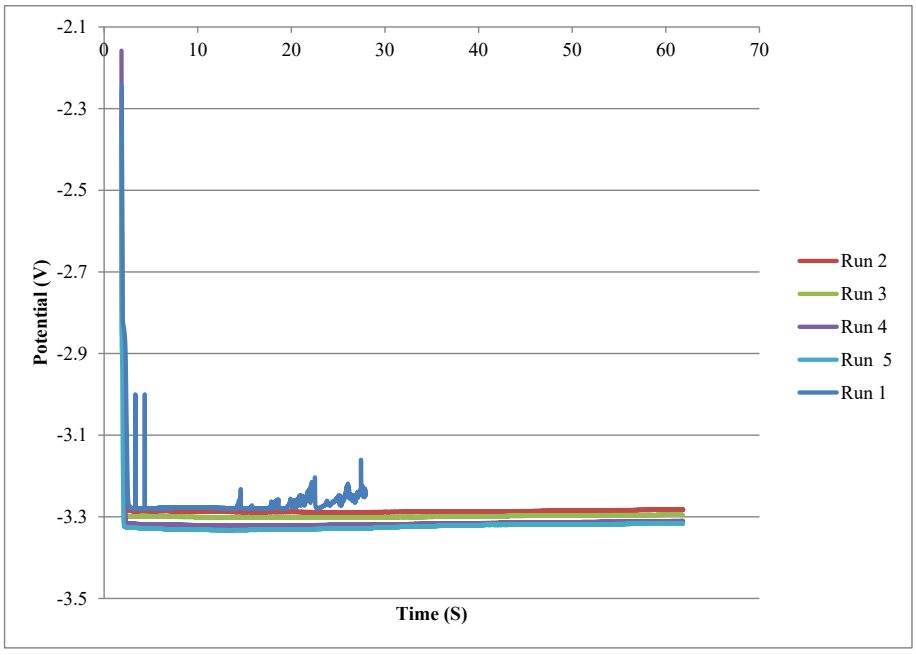

Fig. 3. Experimental Potential (V) versus time (s)of Runs 1–5, 773 K, 0.6 A, Surface Areas: (0.556, 0.0483, 0.410, 0.337,0.265 cm^2), W Working Electrode, Ag/AgCl working electrode adjusted for Cl^-/Cl reference electrode.

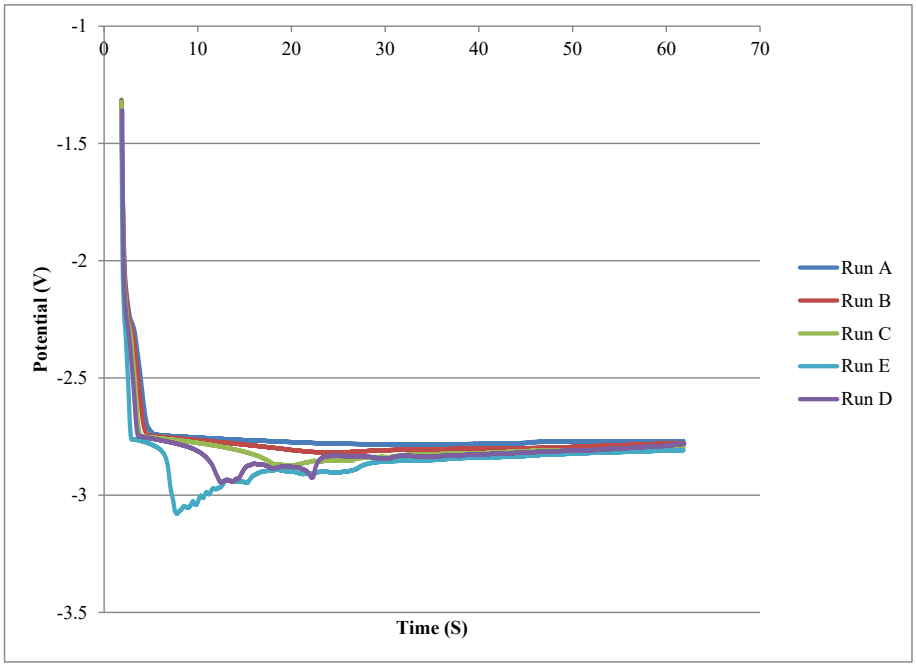

Fig. 4. Experimental Potential (V) versus time (s) of Runs A-E, 773 K, 0.1 A, Surface Areas: (0.556, 0.0483, 0.410, 0.337,0.265 cm^2), W Working Electrode, Ag/AgCl working electrode adjusted for Cl^-/Cl reference electrode.

Run 4 as there is no deposit present and that in the cell with a total charge of 36 Coulombs passed a total of 0.37 mmol of electrons deposited at the cathode but only 0.106 milliequivalents are measured to have deposited indicating that the much of the metal is missing. This 0.37 mmol of electrons deposited is also reflected by the results of the mass deposition simulations of what is equal to 0.37 milliequivalents. The experimental analytical result is difficult to compare to quantitative computational results, but it can be compared to expected qualitative conclusions. A qualitative conclusion being that with increased current density the total mass of Li codeposited increases as well which is an expected result and is reflected in the experimental results presented here.

A plot of the ratio of the experimentally measured and modeled Gd/U ratio of the deposited metals at the cathode versus current density is seen in Fig. 7. As seen in this plot, with increasing current density, there is an increase in the ratio of Gd to U. This is expected because as current density increases, its value exceeds the limiting current density of U by a greater amount with each increase. With

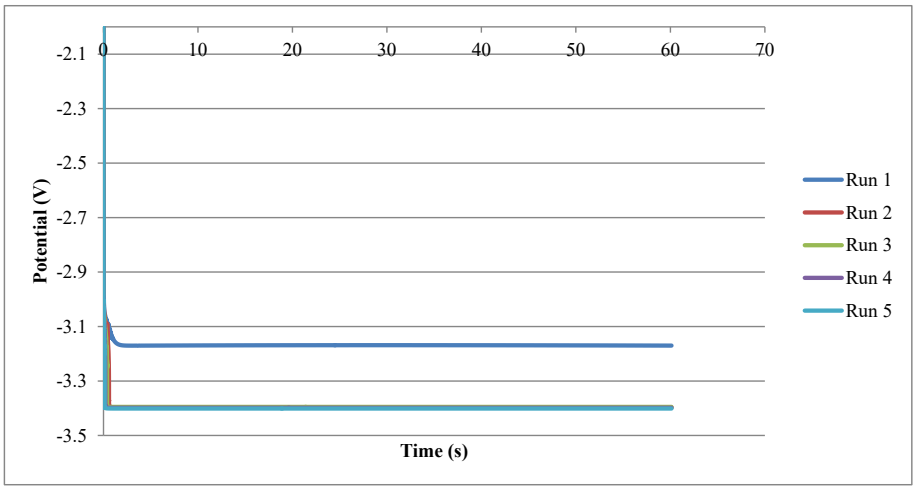

Fig. 5. Computational Potential (V) versus time (s) of Runs 1–5, 773 K, 0.6 A, Surface Areas: (0.556, 0.0483, 0.410, 0.337,0.265 cm^2), W Working Electrode, Ag/AgCl working electrode adjusted for Cl^-/Cl reference electrode.

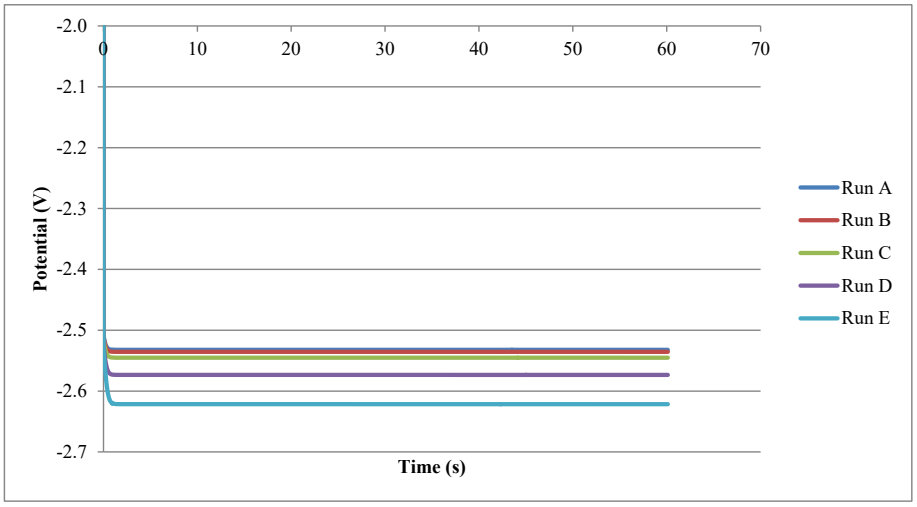

Fig. 6. Calculated Potential (V) versus time (s) of Runs A-E, 773 K, 0.1 A, Surface Areas: (0.556, 0.0483, 0.410, 0.337,0.265 cm^2), W Working Electrode, Ag/AgCl working electrode adjusted for Cl^-/Cl reference electrode.

Table 2
Composition of Salt Samples. Samples taken before an experiment are labeled with i, while samples taken after an experiment are labeled with f.

Sample	Sample wt.	Gd (wt%)	U (wt%)	Li (w%)	K (wt%)
1-i	0.0845	1.865	0.794	7.695	28.588
1-f	0.0522	1.803	0.829	7.340	28.596
2-f	0.043	1.940	0.782	7.978	28.570
3-f	0.0591	1.807	0.722	7.547	28.627
4-f	0.0571	1.805	0.728	7.340	28.625
5-f	0.0596	1.972	0.752	7.298	28.569
A-f	0.0342	1.948	0.848	8.225	28.548
B-f	0.0442	2.019	0.891	8.417	28.514
C-f	0.049	1.981	0.850	8.192	28.538
D-f	0.0521	1.945	0.879	7.992	28.540
E-f	0.1076	1.863	0.844	7.625	28.574

each increasing excess of the limiting current density, the greater fraction of the current applied to the transport of the Gd until it meets a limit dependent mass transport qualities of each species in the salt and the current density exceeds the sum of both the limiting current densities of both the U and Gd resulting in the demonstrated codeposition of Li. The trends seen experimentally are reflected by the calculated results illustrating the potential efficacy of the use of ERAD as predictive tool of failure modes and codeposition scenarios. Specifically, ERAD demonstrates that it can predict the effect of the change of a significant parameter, in this case current density, on the nature of the deposit, Gd/U ratio, for use in further identified failure modes such temperature variations or change cathodic and anodic properties.

At the higher current density operations of runs 1–5, the ERAD calculations are able to calculate specific data trends obtained with experimental measurements. Specifically it calculates average operating potentials that are indicative of the codeposition of U, Gd, and Li at the cathode. There is some difference at very early times in each run, but that may be due to nucleation effects that are not addressed at all in ERAD. However ERAD is able to model the average steady state potential that eventually develops in the experimental system. Thus from the perspective of SBS, ERAD is useable assuming that the average potential is the signal to be integrated into a systems framework. This is certainly the case, since nucleation is only the very beginning of each electrorefining run and represents a tiny fraction of the total run time.

Table 3
ICP-MS results of experimentally measured cathode deposits.

Run	Current (A)	Current Density	Deposited Gd (mg)	Deposited U (mg)	Deposited Li (mg)	Total Deposit (mg)	Gd/U Mass Ratio
1	0.6	0.41	1.75	1.49	0.431	3.66	1.18
2	0.6	0.47	4.22	2.14	1.10	7.46	1.98
3	0.6	0.55	3.86	1.47	1.90	7.23	2.63
4	0.6	0.66	7.46	3.10	0	10.56	2.41
5	0.6	0.82	4.70	1.85	3.48	10.03	2.54
A	0.1	0.069	0.72	2.09	0	2.81	0.34
B	0.1	0.078	0.13	2.08	0	2.22	0.07
C	0.1	0.092	0.95	1.14	0	2.09	0.83
D	0.1	0.11	0.81	1.57	0	2.38	0.52
E	0.1	0.14	0.77	1.32	0	2.09	0.58

Table 4
Computational mass deposition results of simulations of experiments.

Run	Current (A)	Current Density	Deposited Gd (mg)	Deposited U (mg)	Deposited Li (mg)	Gd/U
1	0.6	0.41	12.8	10.2	1.00E-06	1.26
2	0.6	0.47	11.5	9.39	2.54E-01	1.23
3	0.6	0.55	10.6	7.65	5.17E-01	1.39
4	0.6	0.66	8.32	5.94	9.72E-01	1.40
5	0.6	0.82	6.72	4.84	1.28E+00	1.39
A	0.1	0.069	0	4.94	1.00E-06	0.000
B	0.1	0.078	0	4.94	1.00E-06	0.000
C	0.1	0.092	0	4.94	1.00E-06	0.000
D	0.1	0.11	0	4.94	1.00E-06	0.000
E	0.1	0.14	0	4.94	1.00E-06	0.000

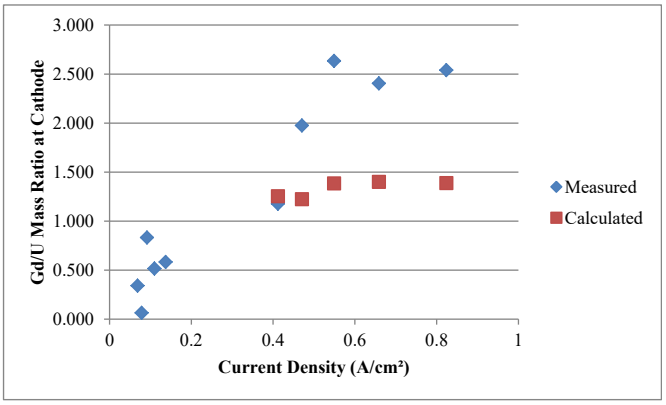

Fig. 7. Plot of Gd/UMass ratio versus current density (A/cm^2) for measured and calculated cathode depositions.

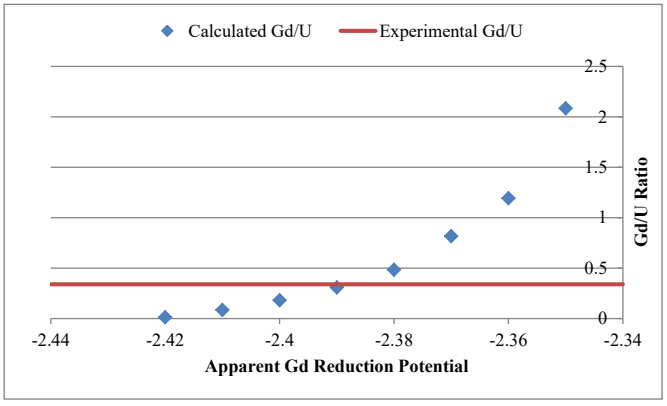

Fig. 8. Example optimization of apparent Gd reduction potential for run A (0.1 A, surface area: 0.556 cm^2).

Comparing the results from the experiments and ERAD simulations for the lower current density operations, Runs A-E, the differences are apparent. Potential results demonstrate that for the low current density runs that the computational calculations are less negative and the cell operates at a potential where only U is deposited at the cathode while the potentials from the experimental operations indicate that the operating potential will involve the codeposition of U and Gd. The resulting deposits reflect this significant difference in the nature of the operating potential as there is a noticeable codeposition that changes with changing current density for the actual experiments while the simulations result in the same mass of U deposit for the same operation. Thus, for lower current density operations and those in which are derived from the start of the slope of the Gd reduction peak of CV curve will not produce a modeled codeposition in ERAD by itself. To best model the conditions of the cell, an optimization of the input parameters, such as the electrochemical data input in it as well as changes in cathode surface area as a result of removal of salt and metal over time from the cell, is required to best predict trends utilizing ERAD. An example of this optimization process is seen in Fig. 8. For the case of Run A, the reduction potential of U was held at −2.33 V, and the apparent reduction potential of Gd was run at various incremental values to make it so that the Gd/U ratio calculated matched that which was obtained experimentally. As can be seen, the reduction potential of Gd can be varied to make it that Gd/U match by making the ΔV between the Gd and U smaller. However, the extent for the case of this operation is a ΔV of only ~0.06 V which is substantially smaller than what is expected by known electrochemical data of Gd and U reduction potentials in LiCl–KCl salt. Thus, a single parameter such as the reduction potential should not be the focus of the optimization, but should include other electrochemical parameters that contribute to transport e.g. standard exchange current density and diffusion coefficient. This focus on these fundamental parameters needs to be applied in subsequent low current calculations in ERAD.

Higher current density operations illustrate that ERAD can

produce predictions of off normal events that are reflected in results from experimental operations. The inputs can be optimized to visualize the trends seen in the lower current density operations experimentally and best improve the model when analyzing future failure mode scenarios computationally allowing for the confirmation of the predictions of safeguards relevant failure modes.

For all sets of runs, the mass transport calculations of ERAD calculates a greater total mass of metal deposited at the cathode for a given electrorefiner run compared to the experimental. Theoretically, by Faraday's law of electrolysis in the 0.1 A current runs, passing 0.1 A of current for 60 s transfers six coulombs of charge which would result in a theoretical value of 4.94 mg of U depositing at the cathode. This theoretical value is the same as is calculated by ERAD. Thus, ERAD captures from the perspective of its idealized assumptions such as fully developed boundary layer and perfect mixing of salt the theoretical value of the mass deposit at the cathode. The discrepancy between experimental and computational values comes from both these assumptions as well as the likely possibility that some deposits fell off upon removal from the cell as well as during the handling and preparation of the ICP-MS samples.

From the perspective of utilizing ERAD to model SBS related off-normal scenarios, ERAD may be adequate from the perspective of expected reference electrode signals and calculating cathode deposits. Absolute values to not closely match those measured from experiments, but the trends are consistent. ERAD successfully predicts the onset of co-deposition of metals, allowing it to simulate various scenarios involving U, Pu, and minor actinides. Thus, ERAD is able to predict the trends demonstrated by the experiments and be utilized for determining the validity of postulated failure modes. Without optimizing its input parameters, it ERAD should not be expected to generate accurate predictions for potentials and masses of deposited metals. Rather it can be used to determine relationships and trends to guide development of safeguards methods and signatures for off-normal operations.

5. Conclusions

Alternate methods for safeguarding new reprocessing facilities such as those based on pyroprocessing are being developed utilizing PM methods. These PM methods process data signals from systems of sensors arranged within this facility. By analyzing these signals for perturbations from normal operation, the nature of operation whether it is normal or anomalous can be concluded. One major PM method, SBS, has been investigated primarily through computational methods utilizing models of both the unit operations equipment and the sensors. This study investigated the validity of the assumptions of the model of the ER equipment known as ERAD.

This study was performed by performing multiple experimental runs on a selected off-normal occurrence–that of a change in cathode surface area resulting in greater current density due to the jamming or malfunction of the cathode in the ER. These results demonstrated that codeposition will occur and will often match the predictions made from theory in terms of the changes of species partial currents and the ratio of mass deposits at the cathode. Both experimental and computational results demonstrate that with increased current densities the ratio of U/Gd increases demonstrating that ERAD possesses the ability to determine trends in failure mode scenarios that are also seen in experimental results. In addition, the trends with regards to change in potential with increasing current density are observed to be the same with both computed and experimental analysis. This demonstrates that ERAD can be utilized to determine qualitative failure mode trends, but still require improvements in application.

In particular, ERAD requires improvements with regards to electrochemical transport and thermodynamic calculations that account for non-steady state conditions. In addition, an optimization of parameters and improvements to modeling of growth on the cathode has been demonstrated to be of importance in the further use of ERAD as applied to failure mode related problems. With these improvements, off-normal condition identification and simulation for SBS will be significantly improved and can improve confidence in terms of the analysis of failure mode effects and the viability of their impact on a modeled system.

Declaration of competing interest

The authors declare that they have no known competing financial interests or personal relationships that could have appeared to influence the work reported in this paper.

Acknowledgements

The authors would like to acknowledge Il Soon Hwang and Man-Sung Yim for providing us and allowing us to use ERAD, and Riley Cumberland for his development of ERAD from the original REFIN code. The authors would also like to acknowledge the Department of Energy- Nuclear Energy's (DOE-NE) Nuclear Energy University Program (NEUP) whose funding assisted in the development of laboratory capabilities utilized for this work.

Appendix A. Supplementary data

Supplementary data to this article can be found online at https://doi.org/10.1016/j.net.2020.02.005.

References

[1] H. Lee, G. Park, J.-W. Lee, K.-H. Kang, J.-M. Hur, J.-G. Kim, S.K.-T. Paek, I.-J. Cho, Current status of pyroprocessing development at KAERI, Sci. Technol. Nucl. Install. 43 (4) (2011) 317–328.
[2] B. Cipiti, F. Duran, B. Key, Y. Liu, I. Lozano, R. Ward, Modeling and Design of Integrated Safeguards and Security for an Electrochemical Reprocessing Facility, Sandia National Laboratories, Albuquerque, 2012.
[3] International Atomic Energy Agency, IAEA Safeguards Glossary, IAEA, Vienna, 2001.
[4] T. Burr, etal, Roles for process monitoring in nuclear safeguards at aqueous reprocessing plants, J. Nucl. Mater. Manag. 40 (2) (2012) 42–52.
[5] T. Burr, M. Hamada, C. Orton, Data-driven versus period-driven change detection for process monitoring, in: Proceeding of the 53rd Annual Institute for Nuclear Materials Management Meeting, 2012. Orlando.
[6] P. Lafreniere, D. Rappleye, R. Hoover, M. Simpson, E. Blandford, Application of signature- based safeguards to electrorefining and the ingot casting process, Nucl. Technol. 189 (2) (2015) 173–185.
[7] H.E. Garcia, M.F. Simpson, W.-C. Lin, T.-S. Yoo, R.B. Carlson, Detecting Proliferation Activities via System-Centric Integration and Interpretation of Multi-Modal Data Collected from a System of Sensors, Idaho National Labs, Idaho Falls, 2013.
[8] M.F. Simpson, D. Rappleye, E.D. Blandford, H. Garcia, Signature based safeguards alternative to nuclear material accountancy, in: Annual Institute for Nuclear Materials Management Meeting, 2014. Atlanta.
[9] P. Lafreniere, R. Hoover, E. Blandford, Determination of pyroprocessing cathode processor failure modes and intregation into a signature-based safeguards (SBS) framework, in: Proceeding of INMM Meeting, 2014. Atlanta.
[10] P. Lafreniere, D. Rappleye, R. Hoover, M. Simpson, E. Blandford, Modeling non-destructive assay based signatures for application to safeguarding pyroprocessing, in: Proceedings of ICAPP, 2014. Charlotte.
[11] R. Cumberland, M.-S. Yim, Development of a 1D transient electrorefiner model for pyrprocess simulations, Transactions of the American Nuclear Society, Washington D.C., 2011.
[12] J. Lee, Y. Kang, S. Hwang, H. Lee, E. Kim, S. Park, Assesment of a hihg-throughput electrorefining concept for a spent metallic nuclear fuel-I: computational fluid dynamics analysis, Nucl. Technol. 162 (1) (2008) 107–116.
[13] R. Cumberland, 1D and 3D Simulation of Electrochemical Behavior of U/UCl3 and Pu/PuCl3 in Molten Salt Systems, Thesis, Korean Advanced Institute of Science and Technology, Daejon, 2013.